



## Geometrical and spectral study of $\beta$ -skeleton graphs

L. Alonso <sup>\*</sup>

*Max-Planck-Institut für Physik Komplexer Systeme, Nöthnitzer Straße 38, 01187 Dresden, Germany*

J. A. Méndez-Bermúdez <sup>†</sup>

*Departamento de Matemática Aplicada e Estatística, Instituto de Ciências Matemáticas e de Computação, Universidade de São Paulo - Campus de São Carlos, Caixa Postal 668, 13560-970 São Carlos, São Paulo, Brazil  
and Instituto de Física, Benemérita Universidad Autónoma de Puebla, Apartado Postal J-48, Puebla 72570, México*

Ernesto Estrada <sup>‡</sup>

*Institute of Mathematics and Applications (IUMA), University of Zaragoza, Pedro Cerbuna 12, 50009 Zaragoza, Spain  
and ARAID Foundation, Government of Aragon, 50008 Zaragoza, Spain*



(Received 18 July 2019; published 19 December 2019)

We perform an extensive numerical analysis of  $\beta$ -skeleton graphs, a particular type of proximity graphs. In a  $\beta$ -skeleton graph (BSG) two vertices are connected if a proximity rule, that depends of the parameter  $\beta \in (0, \infty)$ , is satisfied. Moreover, for  $\beta > 1$  there exist two different proximity rules, leading to lune-based and circle-based BSGs. First, by computing the average degree of large ensembles of BSGs we detect differences, which increase with the increase of  $\beta$ , between lune-based and circle-based BSGs. Then, within a random matrix theory (RMT) approach, we explore spectral and eigenvector properties of random BSGs by the use of the nearest-neighbor energy-level spacing distribution and the entropic eigenvector localization length, respectively. The RMT analysis allows us to conclude that a localization transition occurs at  $\beta = 1$ .

DOI: [10.1103/PhysRevE.100.062309](https://doi.org/10.1103/PhysRevE.100.062309)

### I. INTRODUCTION

The analysis of spatial networks plays a fundamental role for understanding complex systems embedded in geographical spaces; see [1,2]. Here we study a model which is a generalization of the so-called random neighborhood graphs [3,4], known as  $\beta$ -skeleton graphs, embedded in the unit square. In a  $\beta$ -skeleton graph (BSG) two vertices (points or nodes) are connected by an edge if and only if these vertices satisfy a particular geometrical requirement named a proximity rule. The proximity rule is encoded in the  $\beta$  parameter, which takes values in the interval  $0 < \beta < \infty$ . With the proximity rules we will define below, a fully connected graph is obtained in the limit  $\beta \rightarrow 0$ , while the network becomes a disconnected graph when  $\beta \rightarrow \infty$ .

In particular, BSGs are useful to study geometric complex systems where the connectivity between two items is interfered by the presence of a third one in between them. This is the case, for instance, in granular materials [5], for representing urban street networks [6], as well as for representing fractures in rocks [7], among others.

This work is organized as follows. In Sec. II we introduce the proximity rules needed to construct the BSGs. In fact, for  $\beta > 1$  there exist two different proximity rules, leading to

lune-based and circle-based BSGs. Indeed, our study focuses on a detailed comparison between both. Therefore, we study topological and spectral properties of BSGs by using the average degree, in Sec. III, and by using nearest-neighbor energy-level spacing distribution and the entropic eigenvector localization length, in Sec. IV. Finally, we summarize in Sec. V.

### II. DEFINITIONS OF $\beta$ -SKELETON GRAPHS

For a given set of vertices  $V = \{v_1, v_2, \dots, v_n\}$  on the plane, a Euclidean distance function  $d$ , and a parameter  $0 < \beta < \infty$ , a graph  $G_\beta(V)$ , called a BSG, is defined as follows [3]:

Two vertices  $v_i, v_j \in V$  are connected with an edge iff no point from  $V \setminus \{v_i, v_j\}$  belongs to the neighborhood  $\mathcal{N}(v_i, v_j, \beta)$ , where

(1) For  $0 < \beta \leq 1$ ,  $\mathcal{N}(v_i, v_j, \beta)$  is the intersection of two discs, each with radius

$$r = \frac{d(v_i, v_j)}{2\beta}, \quad (1)$$

having the segment  $v_i v_j$  as a chord. The disk centers are located at

$$c_{\pm} = \frac{v_i + v_j}{2} \mp \frac{R(\pi/2)(v_j - v_i)}{2\beta} (1 - \beta^2)^{1/2}, \quad (2)$$

<sup>\*</sup>lalonso@pks.mpg.de

<sup>†</sup>jmendezb@ifuap.buap.mx

<sup>‡</sup>estrada66@unizar.es

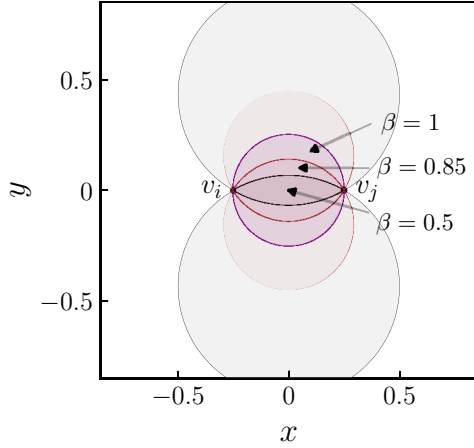


FIG. 1. Examples of neighborhoods  $\mathcal{N}(v_i, v_j, \beta)$  for the vertices  $v_i = (-0.25, 0)$  and  $v_j = (0.25, 0)$  and several values of  $\beta \leq 1$ .

where  $R(\cdot)$  is a rotation matrix and  $v_i$  and  $v_j$  are the coordinate vectors of the corresponding vertices, namely

$$R(\pi/2) = \begin{pmatrix} 0 & -1 \\ 1 & 0 \end{pmatrix}, \quad v_i \equiv \begin{pmatrix} x_i \\ y_i \end{pmatrix}, \quad v_j \equiv \begin{pmatrix} x_j \\ y_j \end{pmatrix}. \quad (3)$$

In Fig. 1 we show some examples of neighborhoods  $\mathcal{N}(v_i, v_j, \beta)$ . We stress that in the limit  $\beta \rightarrow 0$  the neighborhood  $\mathcal{N}$  becomes the straight line joining the vertices  $v_i$  and  $v_j$ , so the network becomes fully connected.

(2) For  $\beta > 1$  there are two proximity rules:

(2a) **Lune-based BSG.** Here  $\mathcal{N}(v_i, v_j, \beta)$  is the intersection of two discs, each with radius

$$r = \frac{\beta d(v_i, v_j)}{2}, \quad (4)$$

whose centers are at

$$c_1 = \frac{\beta}{2} v_i + \left(1 - \frac{\beta}{2}\right) v_j, \quad (5)$$

$$c_2 = \frac{\beta}{2} v_j + \left(1 - \frac{\beta}{2}\right) v_i. \quad (6)$$

In Fig. 2(a) we can see the lunes of influence for different values of  $\beta \geq 1$ . Note that in the limiting case  $\beta \rightarrow \infty$ ,

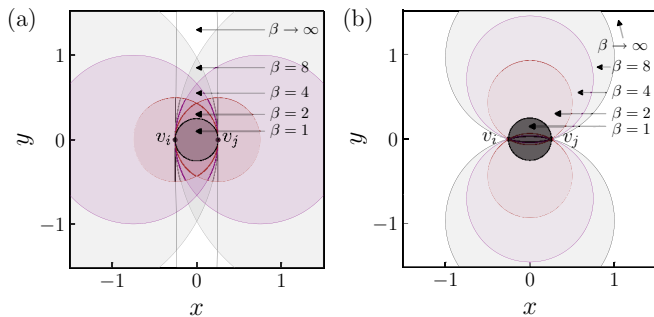


FIG. 2. Examples of (a) lune-based and (b) circle-based neighborhoods  $\mathcal{N}(v_i, v_j, \beta)$  for the vertices  $v_i = (-0.25, 0)$  and  $v_j = (0.25, 0)$  and some values of  $\beta \geq 1$ .

$\mathcal{N}(v_i, v_j, \beta)$  is an infinite strip of width  $|v_i - v_j|$ ; thus, even for very large values of  $\beta$  some connections may exist.

(2b) **Circle-based BSG.** Here  $\mathcal{N}(v_i, v_j, \beta)$  is the union of two discs, with radius given by Eq. (4), that pass through both  $v_i$  and  $v_j$ . The disk centers are located at

$$c_{\pm} = \frac{v_i + v_j}{2} \mp \frac{R(\pi/2)(v_j - v_i)}{2} (\beta^2 - 1)^{1/2}. \quad (7)$$

In Fig. 2(b) we can see the circles of influence for different values of  $\beta \geq 1$ . Note that in the limiting case  $\beta \rightarrow \infty$ ,  $\mathcal{N}(v_i, v_j, \beta)$  is the entire plane; therefore, for large enough values of  $\beta$  the skeleton graph becomes a disconnected graph.

It is worth mentioning that, for  $\beta = 1$ , Eqs. (2), (5), and (7) reduce to the same expression. Indeed, the case  $\beta = 1$  is well known in the literature as Gabriel graph [8] and is called a 1-skeleton graph. Another well known case is  $\beta = 2$ , which is known as relative neighborhood graph [4], in the lune-based formulation, and is typically called a 2-skeleton graph.

### III. RANDOM $\beta$ -SKELETON GRAPHS IN THE UNIT SQUARE

In this work we consider randomly and independently distributed vertices in the unit square. As examples, in Fig. 3 we show BSGs with  $\beta = 0.5$  and  $\beta = 1$  for  $N = 200$ . Note that we have used the same set of randomly distributed vertices in both panels. Here, since  $\beta \leq 1$  the proximity rule is unique. Then, in Fig. 4 we present BSGs for  $\beta = 1.5$  and  $\beta = 2$ . There we consider both the lune-based (left panels) and the circle-based (right panels) proximity rules. We have used the same set of vertices as in Fig. 3. From this figure it is clear that different proximity rules produce quite different networks. In particular, for a fixed value of  $\beta$ , lune-based skeleton graphs show higher connectivity than circle-based skeleton graphs. We will characterize this feature by the use of geometrical and spectral properties below.

#### Average degree

A well known topological measure in graph theory is the degree of a vertex  $k$ , which is the number of edges incident to a given vertex. Here, since we are interested in random BSGs, we will consider the ensemble average degree  $\langle k \rangle$  that we compute by averaging over all vertices of BSGs with fixed parameter pairs  $(N, \beta)$ .

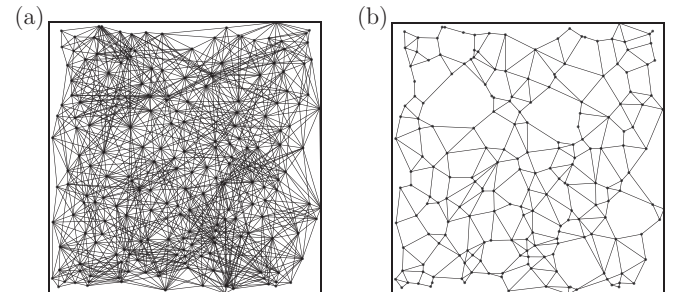


FIG. 3. BSGs with (a)  $\beta = 0.5$  and (b)  $\beta = 1$  for the same set of  $N = 200$  randomly distributed vertices in the unit square.

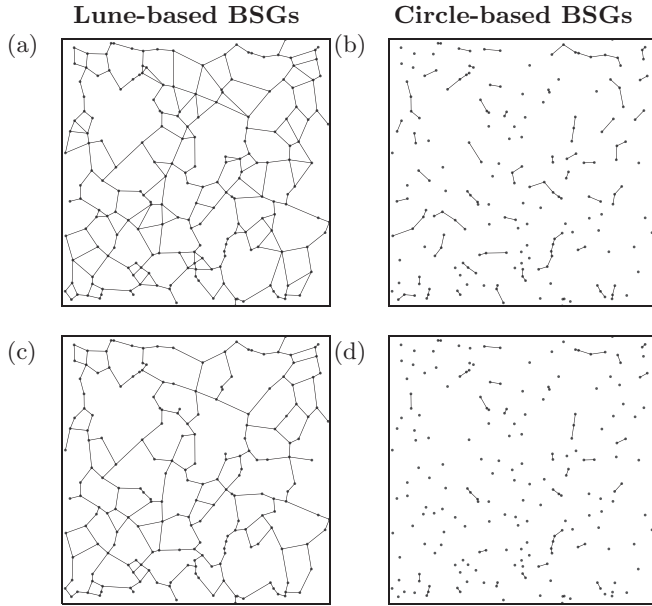


FIG. 4. BSGs with (a), (b)  $\beta = 1.5$  and (c), (d)  $\beta = 2$  for the same set of randomly distributed vertices of Fig. 3. The lune-based (circle-based) proximity rule was used in the left (right) panels.

On the one hand, in Figs. 5 we plot  $\langle k \rangle$  as a function of  $N$  for random BSGs with several values of  $\beta < 1$  (i.e., when only one proximity rule applies). We observe that, for fixed  $\beta$ ,  $\langle k \rangle$  increases for increasing  $N$ . Moreover, for fixed  $N$ ,  $\langle k \rangle$  increases for decreasing  $\beta$ ; this confirms the expected scenario of completely connected networks in the limit  $\beta \rightarrow 0$ .

On the other hand, in Figs. 6 and 7 we also plot  $\langle k \rangle$  as a function of  $N$  but now for random BSGs with  $\beta \geq 1$ . We consider both lune-based (left panels) and circle-based (right panels) proximity rules. For clarity, we group the data in the regimes  $1 \leq \beta < 2$  (Fig. 6) and  $\beta \geq 2$  (Fig. 7). First, let us concentrate on the BSGs constructed with the lune-based proximity rule; see left panels in Figs. 6 and 7. There, we observe three different behaviors for  $\langle k \rangle$ : (i) when  $\beta$  is small,  $\beta < 2$ ,  $\langle k \rangle$  is an increasing function of  $N$ ; (ii) for intermediate

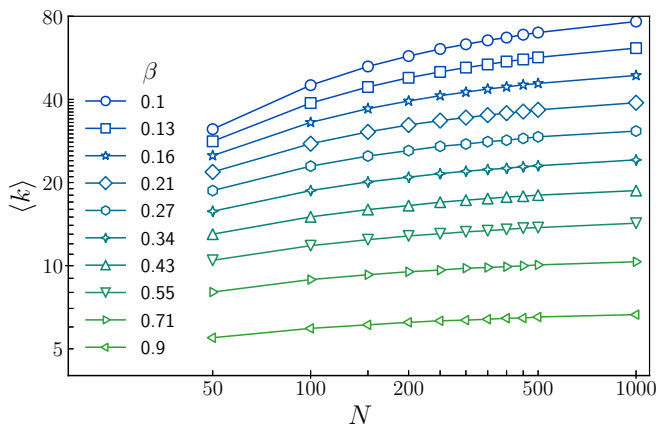


FIG. 5. Average degree  $\langle k \rangle$  as a function of  $N$  for random BSGs with  $\beta < 1$ . Here, the standard deviation error is smaller than the symbol size.

values of  $\beta$ ,  $2 \leq \beta \leq 20$ ,  $\langle k \rangle$  is approximately constant for the values of  $N$  we used in this work; and (iii) when  $\beta$  is large,  $\beta > 20$ ,  $\langle k \rangle$  is a decreasing function of  $N$ . This pattern is also observed for BSGs constructed with the circle-based proximity rule (see right panels in Figs. 6 and 7) but shifted to smaller values of  $\beta$ ; that is,  $\langle k \rangle$  is approximately constant as a function of  $N$  for  $1.5 \leq \beta \leq 4$ .

From the observations above we can conclude that for intermediate values of  $\beta$  (including relative neighbor graphs) the BSGs are very stable graphs in the sense that the average degree remains constant as a function of  $N$ .

Moreover, in Fig. 8(a) we now plot  $\langle k \rangle$  versus  $\beta$  for BSGs constructed with both the lune-based and circle-based proximity rules. From this figure, one can clearly see that  $\langle k \rangle$  is a monotonically decreasing function of  $\beta$ . However,  $\langle k \rangle$  decreases faster with  $\beta$  for the circle-based proximity rule. Also, note that the decrease of  $\langle k \rangle$  as a function of  $\beta$  implies the increase of the number of isolated vertices,  $N_{\text{isolated}}$ , whose average we report in Fig. 8(b). Notice that  $\langle N_{\text{isolated}} \rangle = 0$  when  $\beta < 1$  ( $\beta < 2$ ) for circle-based (lune-based) BSGs; i.e., for those values of  $\beta$  the giant component of the graph contains all vertices.

Therefore, the main difference we can observe between random BSGs constructed with the lune-based and circle-based proximity rules is that in the circle-based case the networks become disconnected for relatively smaller values of  $\beta$  than in the lune-based case; compare Figs. 7(a) and 7(b), left and right panels in Fig. 4, and also the curves in Fig. 8. Indeed, from Figs. 7(b) and 8 it is clear that when  $\beta \geq 100$  it is highly probable to have completely disconnected BSGs when they are constructed following the circle-based proximity rule.

#### IV. RANDOM MATRIX THEORY APPROACH TO $\beta$ -SKELETON GRAPHS

The study of spectral and eigenvector properties of the adjacency matrices of random graphs, by the use of random matrix theory (RMT) measures, is a well known practice; see, e.g., [9–14]. However, here we apply a less widespread approach that considers, in addition, the construction of a RMT ensemble appropriate for the graph under study; see some examples of this approach in Refs. [15–17].

Specifically, we define the RMT ensemble corresponding to the random BSGs as follows. We choose the nonvanishing elements of the adjacency matrices  $\mathbf{A}$  to be statistically independent random variables drawn from a normal distribution with zero mean,  $\langle A_{ij} \rangle = 0$ , and variance  $\langle |A_{ij}|^2 \rangle = (1 + \delta_{ij})/2$ , where  $\delta_{ij}$  is the Kronecker delta. Therefore, for graphs with isolated vertices, diagonal random adjacency matrices are obtained, known in RMT as the Poisson ensemble [18]. When the graphs are fully connected, real and symmetric full random adjacency matrices are recovered; known in RMT as the Gaussian orthogonal ensemble (GOE) [18]. Note that in our random BSGs the Poisson ensemble and the GOE are reproduced for  $\beta \rightarrow \infty$  and  $\beta \rightarrow 0$ , respectively. Thus, the random adjacency matrices corresponding to the random BSGs work as an interpolating RMT ensemble that transits from the GOE to the Poisson ensemble by increasing  $\beta$ .

The use of randomly weighted adjacency matrices (instead of the standard binary ones) (i) allows the use of RMT

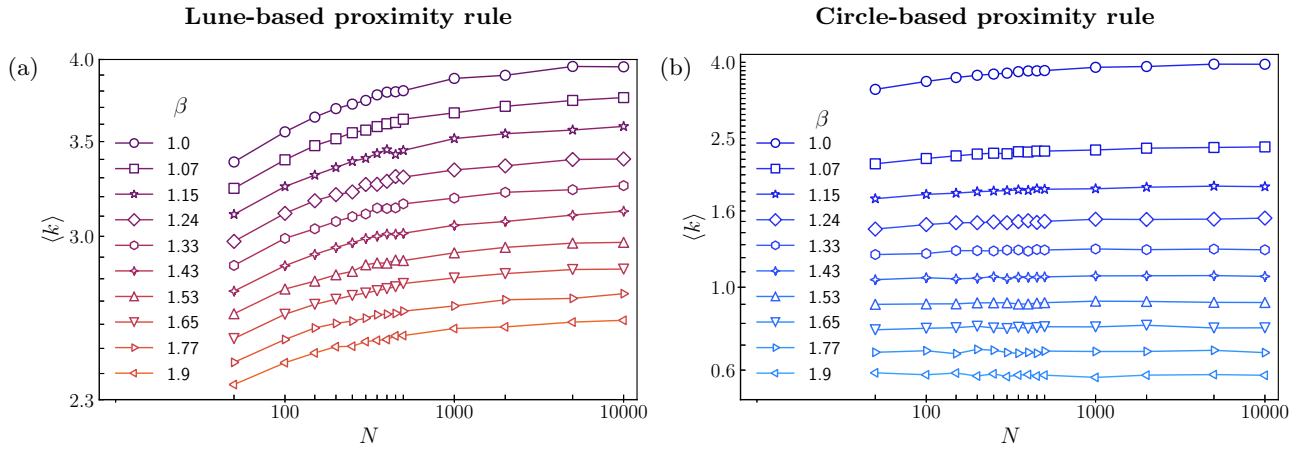


FIG. 6. Average degree  $\langle k \rangle$  as a function of  $N$  for random BSGs with  $1 \leq \beta < 2$ . In both panels the standard deviation error is smaller than the symbol size.

predictions in the proper limits and (ii) avoids handling of null matrices for graphs with isolated vertices, so it is possible to numerically approach the limit  $\beta \rightarrow \infty$ . Moreover, it is important to stress that the topology of the random BSGs, as defined in Secs. II and III, is not affected by adding weights to the corresponding adjacency matrices.

Therefore, below we use exact numerical diagonalization to obtain the eigenvalues  $\lambda^m$  and eigenvectors  $\Psi^m$  ( $m = 1, \dots, N$ ) of large ensembles of randomly weighted adjacency matrices characterized by  $\beta$  and  $N$ .

**A. Spectral properties**

In order to characterize the spectra of random BSGs, we use the nearest-neighbor energy level spacing distribution  $P(s)$  [18], a widely used tool in RMT. For  $\beta \rightarrow \infty$ , i.e., when the vertices in the random BSGs are mostly isolated, the corresponding randomly weighted adjacency matrices are almost diagonal and, regardless of the size of the graph,  $P(s)$  should be close to the exponential distribution,

$$P(s) = \exp(-s), \tag{8}$$

which is better known in RMT as the Poisson distribution. In the opposite limit,  $\beta \rightarrow 0$ , when the BSGs are fully connected, the randomly weighted adjacency matrices become members of the GOE and  $P(s)$  closely follows the Wigner-Dyson distribution,

$$P(s) = \frac{\pi}{2} s \exp\left(-\frac{\pi}{4} s^2\right). \tag{9}$$

Thus, for a fixed graph size  $N$ , by increasing  $\beta$  from zero to infinity, the shape of  $P(s)$  is expected to evolve from the Wigner-Dyson distribution to the Poisson distribution. Moreover, for a fixed value of  $\beta$ , the increase in the density of vertices  $N$  also produces changes in the shape of  $P(s)$ . In Fig. 9 we explore both scenarios.

We construct histograms of  $P(s)$  from  $N/2$  unfolded spacings [18],  $s_m = (\lambda^{m+1} - \lambda^m)/\Delta$ , around the band center of a large number of graph realizations (such that all histograms are constructed with  $5 \times 10^5$  spacings). Here,  $\Delta$  is the mean level spacing computed for each adjacency matrix. Then, Fig. 9 presents histograms of  $P(s)$  for the randomly weighted adjacency matrices of random BSGs: In Fig. 9(a) the graph

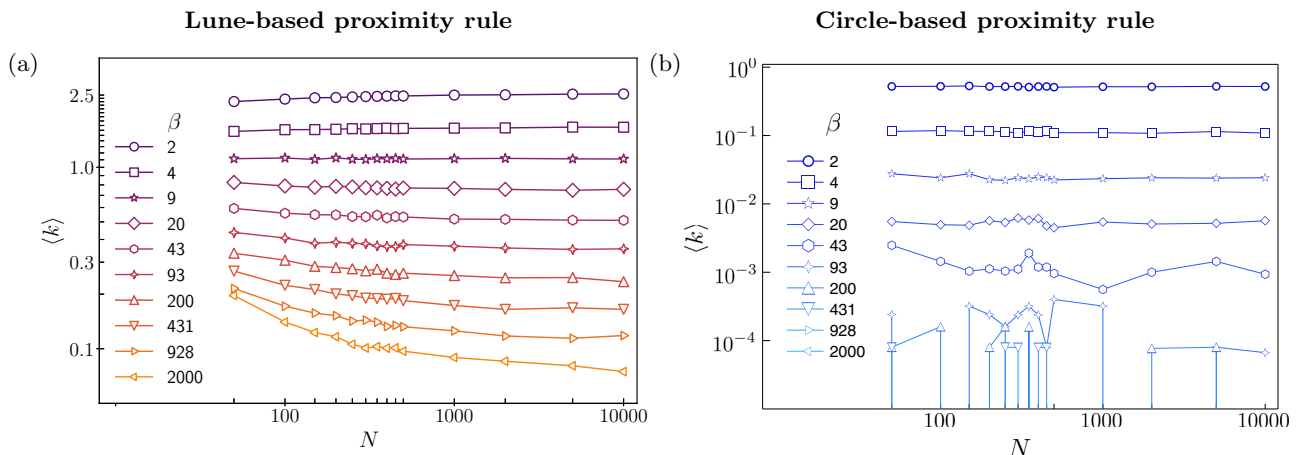


FIG. 7. (a), (b) Average degree  $\langle k \rangle$  as a function of  $N$  for random BSGs with  $\beta \geq 2$ . In (a) the standard deviation error is smaller than the symbols size.

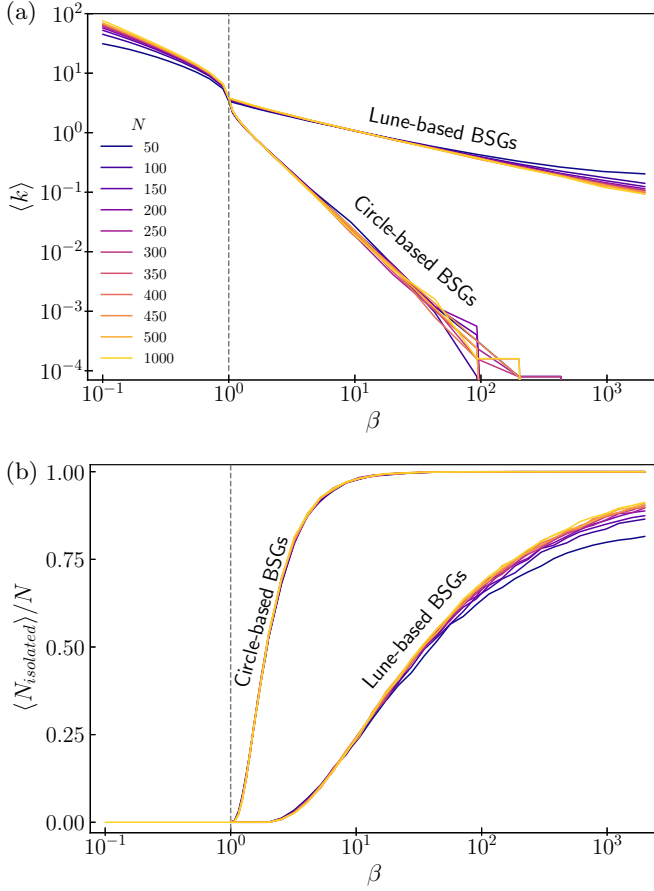


FIG. 8. (a) Average degree  $\langle k \rangle$  as a function of  $\beta$  for random BSGs for several values of  $N$ . (b) Fraction of isolated nodes (normalized to  $N$ ),  $\langle N_{\text{isolated}} \rangle / N$ , as a function of  $\beta$ . In both panels the lune-based and circle-based proximity rules are reported.

size is fixed to  $N = 10^2$  and  $\beta$  takes the values 0.1, 0.9, 1, and 10. In this figure we observe a complete transition in the shape of  $P(s)$  from the Wigner-Dyson to Poisson distribution functions (also shown as reference) for increasing  $\beta$ . In Fig. 9(b) the parameter  $\beta$  is set to 1 (Gabriel graph) while  $N$  increases from 6 to  $10^4$ . Here, in contrast to Fig. 9(a), we do not observe a complete transition from Wigner-Dyson to Poisson in the shape of  $P(s)$ . From Fig. 9(b) one may expect that by decreasing further the number of vertices  $N$  the Wigner-Dyson shape could emerge; however, this is not the case, as shown in Fig. 10. There we observe that for  $N < 6$  the  $P(s)$  becomes symmetric with respect to  $s = 1$ . It is important to stress that we have not observed this shape for the  $P(s)$  before. Indeed, in other random network models embedded in the plane, such as random regular graphs and random rectangular graphs (RRGs) (for the definition and general properties of RRGs the reader is referred to [19]), we did observe the full transition from Wigner-Dyson to Poisson for the  $P(s)$  as a function of the density of vertices for a fixed value of the proximity rule parameter [15].

Now, in order to characterize the shape of  $P(s)$  for random BSGs we use the Brody distribution [20,21]

$$P(s) = (\mu + 1)a_\mu s^\mu \exp(-a_\mu s^{\mu+1}), \quad (10)$$

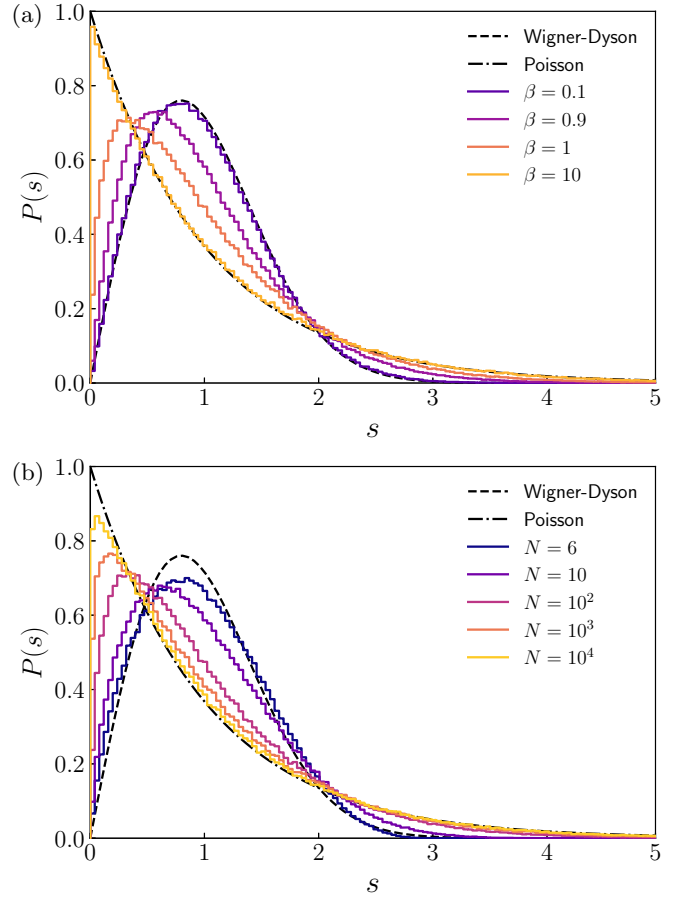


FIG. 9. Nearest-neighbor energy level spacing distribution  $P(s)$  for random BSGs with (a) [(b)]  $N = 10^2$  [ $\beta = 1$ ] and several values of  $\beta$  [ $N$ ]. Here we use the lune-based proximity rule to construct the BSGs. Dash-dotted and dashed lines correspond to the Poisson and Wigner-Dyson distribution functions given by Eqs. (8) and (9), respectively.

where  $a_\mu = \Gamma[(\mu + 2)/(\mu + 1)]^{\mu+1}$ ,  $\Gamma(\cdot)$  is the gamma function, and  $\mu$ , known as Brody parameter, takes values in the range  $[0,1]$ . Equation (10) was originally derived to provide

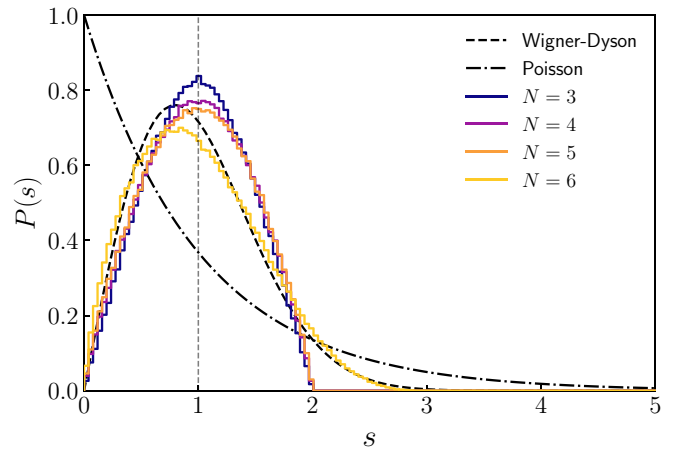


FIG. 10. Nearest-neighbor energy level spacing distribution  $P(s)$  for random BSGs with  $\beta = 1$  and  $N \leq 6$ . Vertical dashed line at  $s = 1$  is plotted to guide the eye.

an interpolation expression for  $P(s)$  in the transition from Poisson to Wigner-Dyson distributions, serving as a measure for the degree of mixing between Poisson and GOE statistics. In fact,  $\mu = 0$  and  $\mu = 1$  in Eq. (10) produce Eqs. (8) and (9), respectively. In particular, as we show below, the Brody parameter will allow us to identify the onset of the localization transition for random BSGs. It is also relevant to mention that the Brody distribution has been applied to study other complex networks models; see, e.g., [9–16]. In fact, we found that Eq. (10) provides excellent fittings to the histograms of  $P(s)$  of random BSGs. For example, the fittings to the histograms in Fig. 9(a) [Fig. 9(b)] (not shown to avoid figure saturation) provide  $\mu(\beta) = 0.953(0.1)$ ,  $0.624(0.9)$ ,  $0.276(1)$ , and  $0.002(10)$  [ $\mu(N) = 0.872(6)$ ,  $0.645(10)$ ,  $0.316(10^2)$ ,  $0.145(10^3)$ , and  $0.0468(10^4)$ ]. It is important to remark that for  $N \leq 5$  the  $P(s)$  cannot be fitted by the Brody distribution (see Fig. 10), therefore we will not consider small graph sizes in our analysis below.

Thus we now perform a systematic study of the Brody parameter  $\mu$  as a function of the parameters  $\beta$  and  $N$  of the BSGs. To this end, we construct histograms of  $P(s)$  for a large number of parameter combinations to extract the corresponding values of  $\mu$  by fitting them using Eq. (10). Figure 11 reports  $\mu$  versus  $\beta$  for five different graph sizes for both lune-based and circle-based proximity rules. Notice that in all cases the behavior of  $\mu$  is similar for increasing  $\beta$ : For small  $\beta$  (i.e.,  $\beta \leq 0.1$ )  $\mu$  is approximately constant and equal to 0.96; then  $\mu$  decreases fast for  $\beta$  approaching 1; and finally, for  $\beta > 1$ ,  $\mu$  continues decreasing but slowly when  $\beta$  is further increased. For large  $\beta$  (i.e.,  $\beta > 10$ ) and large  $N$ ,  $\mu \approx 0$ .

Indeed, from Fig. 11 we can conclude that our model of random BSGs undergoes a clear and sharp transition at  $\beta = 1$  from a regime very close to the GOE regime (mostly connected vertices),  $\mu \approx 0.96$ , to the Poisson regime (mostly isolated vertices),  $\mu \approx 0$ , as a function of  $\beta$ . What is remarkable is that this delocalization-to-localization transition seems to be independent of the density of vertices  $N$ ; in fact, the larger the value of  $N$  the sharper the transition at  $\beta = 1$  is. It is interesting to recall that we have also identified

a delocalization-to-localization transition in random regular graphs as a function of the proximity rule parameter [15]; however, for that model the transition is rather smooth and importantly depends on the density of vertices. In addition, in the inset of Fig. 11(a) we present the values of  $\mu$  for increasing  $N$  for Gabriel graphs where we include the case  $N = 4000$ .

The main difference we can observe between random BSGs constructed with the lune-based and circle-based proximity rules is that the Poisson limit is approached faster in the circle-based case, which was already expected from the analysis of the average degree of the previous Subsection since there it was shown that circle-based BSGs become completely disconnected for relatively smaller values of  $\beta$ .

## B. Eigenvector properties

The term “localization transition” we used in the previous subsection to describe the sharp decrease of  $\mu$  at  $\beta = 1$  implies that we expect the eigenvectors of the adjacency matrices of BSGs to be mostly localized for  $\beta > 1$ . In the following we verify this statement.

To measure quantitatively the spreading of eigenvectors in a given basis, i.e., their localization properties, two quantities are mostly used: (i) the information or Shannon entropy  $S$  and (ii) the inverse participation number  $I_2$ . Indeed, both have been widely used to characterize the eigenvectors of the adjacency matrices of random network models. For the eigenvector  $\Psi^m$ , associated with the eigenvalue  $\lambda^m$ , they are given as

$$S^m = - \sum_{n=1}^N |\Psi_n^m|^2 \ln |\Psi_n^m|^2 \quad (11)$$

and

$$I_2^m = \sum_{n=1}^N |\Psi_n^m|^4. \quad (12)$$

These measures provide the number of main components of the eigenvector  $\Psi^m$ . Moreover,  $S^m$  allows one to compute the so-called entropic eigenvector localization length [22]

$$\ell = N \exp[-(S_{\text{GOE}} - \langle S^m \rangle)], \quad (13)$$

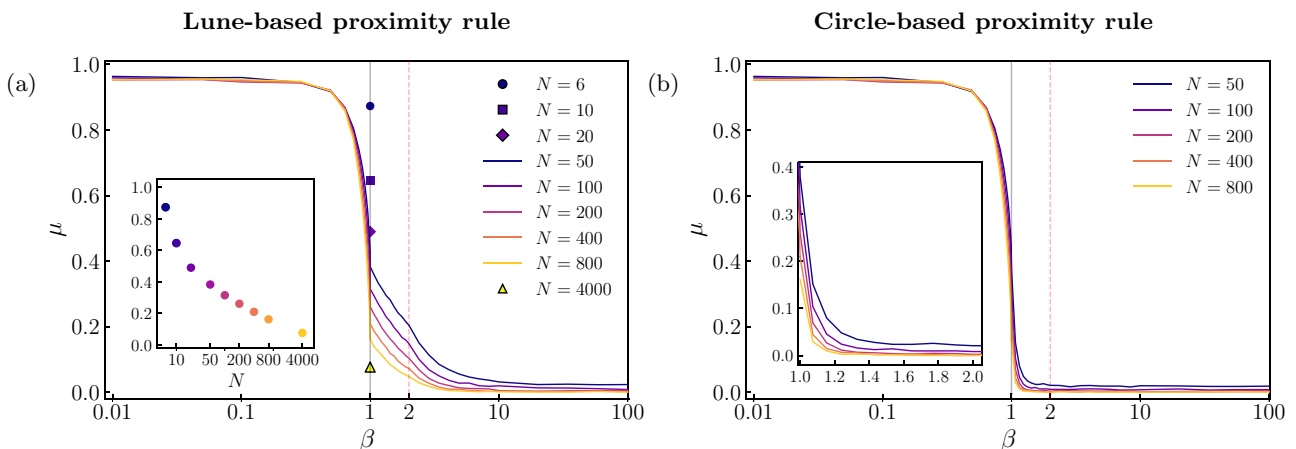


FIG. 11. Brody parameter  $\mu$  as a function of  $\beta$  for several values of  $N$  for (a) lune-based and (b) circle-based random BSGs. Vertical lines in the main panels indicate Gabriel graphs ( $\beta = 1$ ) and relative neighbor graphs ( $\beta = 2$ ). The inset in (a) shows  $\mu$  vs  $N$  for  $\beta = 1$  (Gabriel graphs). The inset in (b) is an enlargement of the main panel in the interval  $1 \leq \beta \leq 2$ .

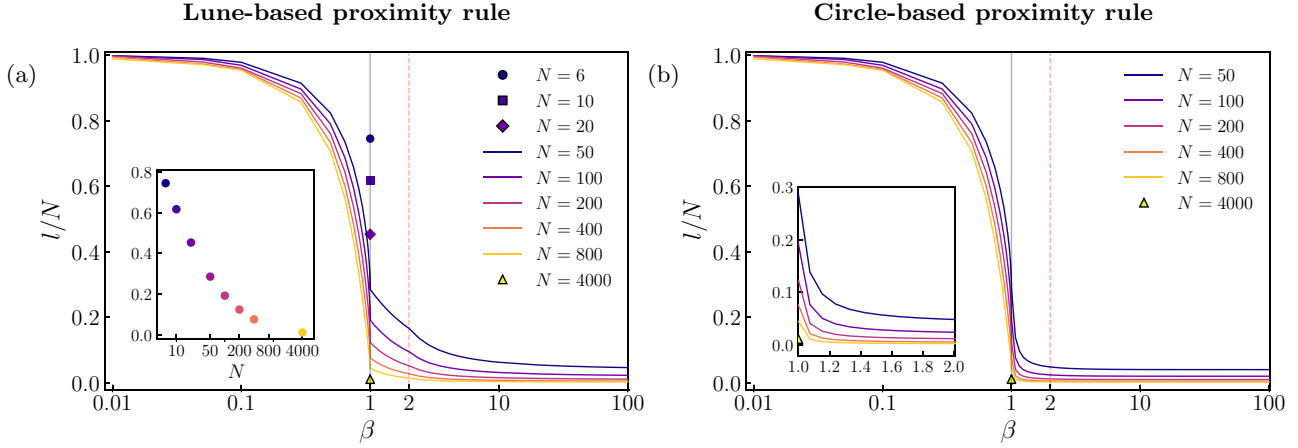


FIG. 12. Entropic eigenvector localization length  $\ell$  (normalized to  $N$ ) as a function of  $\beta$  for several values of  $N$  for (a) lune-based and (b) circle-based random BSGs. Vertical lines in the main panels indicate Gabriel graphs ( $\beta = 1$ ) and relative neighbor graphs ( $\beta = 2$ ). The inset in (a) shows  $\ell$  vs  $N$  for  $\beta = 1$  (Gabriel graphs). The inset in (b) is an enlargement of the main panel in the interval  $1 \leq \beta \leq 2$ .

where  $S_{\text{GOE}}$  is the average entropy of a random eigenvector with Gaussian distributed amplitudes (i.e., an eigenvector of the GOE), which is given by [23]

$$S_{\text{GOE}} = \psi\left(\frac{N}{2} + 1\right) - \psi\left(\frac{3}{2}\right). \quad (14)$$

Above,  $\langle \cdot \rangle$  denotes average and  $\psi(\cdot)$  is the digamma function;  $S_{\text{GOE}} \approx \ln(N/2.07)$  for large  $N$ .

We average over all eigenvectors of an ensemble of adjacency matrices of size  $N$  to compute  $\langle S^m \rangle$ , such that for each combination  $(N, \beta)$  we use  $5 \times 10^5$  eigenvectors. With definition (13), when  $\beta \rightarrow \infty$ , since the eigenvectors of the adjacency matrices of BSGs have only one main component with magnitude close to 1,  $\langle S^m \rangle \approx 0$  and  $\ell \approx N \exp[-S_{\text{GOE}}] \approx \text{const.} \approx 2.07$ . On the other hand, for  $\beta \rightarrow 0$ ,  $\langle S^m \rangle \approx S_{\text{GOE}}$  and the fully chaotic eigenvectors extend over the  $N$  available vertices of the BSG, so  $\ell \approx N$ .

Therefore, in Fig. 12 we plot  $\ell/N$  as a function of  $\beta$  for random BSGs of sizes ranging from  $N = 50$  to 800.

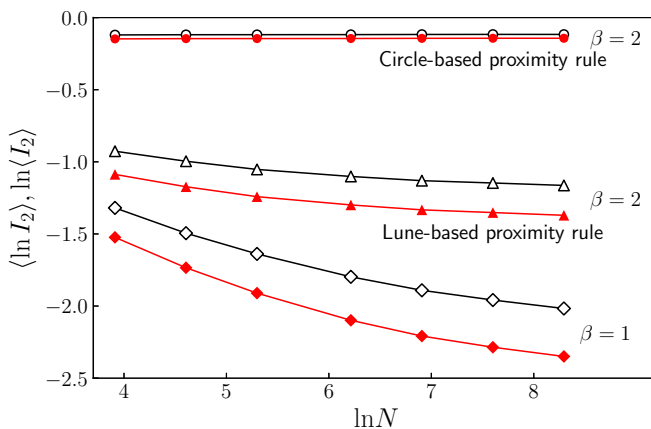


FIG. 13.  $\langle \ln I_2 \rangle$  (red full symbols) and  $\ln \langle I_2 \rangle$  (black empty symbols) as a function of  $\ln N$  for Gabriel graphs (diamonds) and relative neighborhood graphs (triangles and circles for lune-based proximity rule and circle-based proximity rule, respectively).

We consider both lune-based [Fig. 12(a)] and circle-based [Fig. 12(b)] proximity rules. As for the Brody parameter vs  $\beta$  (see Fig. 11), here we clearly observe a sharp transition from delocalized to localized eigenvectors at  $\beta = 1$ . Additionally, in the inset of Fig. 12(a) we report  $\ell/N$  vs  $N$  for  $\beta = 1$ . There we can clearly see the GOE ( $\ell/N \sim 1$ ) to Poisson ( $\ell/N \sim 0$ ) transition in the eigenvector properties of Gabriel graphs, also reported through spectral properties, by the use of  $P(s)$ ; see the inset of Fig. 11(b).

Finally, we would like to add that the inverse participation number of the eigenvectors of BSGs shows an equivalent panorama to that reported in Fig. 12 for  $\ell$ , so we do not show it here. Instead, in Fig. 13 we plot  $\langle \ln I_2 \rangle$  and  $\ln \langle I_2 \rangle$  as a function of  $\ln N$  for Gabriel graphs ( $\beta = 1$ ) and relative neighborhood graphs ( $\beta = 2$ ). The nonlinear trend of the curves corresponding to  $\beta = 1$  and  $\beta = 2$  in the lune-based proximity rule rejects the possible existence of a localization transition of the Anderson type where the eigenvectors are multifractal objects characterized by a set of dimensions  $D_q$ , where the correlation dimension  $D_2$  can be extracted from the scalings  $I_2^{\text{yp}} \propto N^{-D_2}$  or  $\langle I_2 \rangle \propto N^{-D_2}$  ( $I_2^{\text{yp}} \equiv \exp(\ln I_2)$  is known as the typical value of  $I_2$ ). See for example Refs. [24–26] where multifractality of eigenvectors has been reported in random graph models. Moreover the independence of both  $\langle \ln I_2 \rangle$  and  $\ln \langle I_2 \rangle$  on  $N$  for  $\beta = 2$  in the circle-based proximity rule confirms that the corresponding eigenvectors are in the localized regime; that is,  $D_2 \approx 0$ .

## V. CONCLUSIONS

In this paper we perform a thorough study of a particular type of proximity graphs known as  $\beta$ -skeleton graphs (BSGs). In a BSG two vertices are connected if a proximity rule, that depends of the parameter  $\beta \in (0, \infty)$ , is satisfied. We explore the two known versions of them: Lune-based and circle-based BSGs.

Our main result is the identification of a delocalization-to-localization transition at  $\beta = 1$  for the eigenvectors of the adjacency matrices of BSGs for increasing  $\beta$ . It is important to stress that the localized phase corresponds to mostly isolated

vertices while the delocalized phase identifies mostly complete graphs; see Fig. 8. We characterize the delocalization-to-localization transition by means of topological and spectral properties; we use the standard average degree as topological measure and, within a random matrix theory approach, the nearest-neighbor energy-level spacing distribution and the entropic eigenvector localization length as spectral measures.

It is important to stress that the delocalization-to-localization transition we report here for the random BSGs is significantly different from the transitions we observed in other random network models and RMT ensembles. While for Erdős-Rényi random graphs [16] and random regular graphs [15] we were able to find a *universal parameter*  $\xi$  (that explicitly depends on  $N$ ) for which the spectral and eigenvector properties of the corresponding graph models are scalable

(i.e. the curves  $\mu$  vs  $\xi$  and  $\ell/N$  vs.  $\xi$ , for different values of  $N$ , fall on top of invariant smooth curves), here, in contrast, the delocalization-to-localization transition curves evolve with the increase of  $N$  towards a nondifferentiable function at  $\beta = 1$ , resembling a thermodynamic phase transition. Therefore, the RMT ensemble we define here, through the randomly weighted adjacency matrices of BSGs, may serve to study and characterize thermodynamic-like phase transitions.

#### ACKNOWLEDGMENTS

J.A.M.-B. thanks support from FAPESP (Grant No. 2019/06931-2), Brazil, and from VIEP-BUAP (Grant No. 100405811-VIEP2019) and Fondo Institucional PIFCA (Grant No. BUAP-CA-169), Mexico.

- 
- [1] M. Barthélémy, Spatial networks, *Phys. Rep.* **499**, 1 (2011).
  - [2] M. Barthelemy, *Morphogenesis of Spatial Networks*, Lecture Notes in Morphogenesis (Springer, Cham, 2018).
  - [3] D. G. Kirkpatrick and J. D. Radke, *A Framework for Computational Morphology* (IBM Thomas J. Watson Research Division, Yorktown Heights, NY, 1984).
  - [4] G. T. Toussaint, The relative neighborhood graph of a finite planar set, *Pattern Recognit.* **12**, 261 (1980).
  - [5] D. S. Bassett, E. T. Owens, K. E. Daniels, and M. A. Porter, Influence of network topology on sound propagation in granular materials, *Phys. Rev. E* **86**, 041306 (2012).
  - [6] T. Osaragi and Y. Hiraga, Street network created by proximity graphs: Its topological structure and travel efficiency, in *Proceedings of the 17th Conference of the Association of Geographic Information Laboratories for Europe on Geographic Information Science (AGILE2014)*, Castellón, Spain, 2014, edited by J. Huerta, S. Schade, and C. Granell (AGILE Digital Editions, Aalborg, 2014), pp. 1–6.
  - [7] E. Estrada and M. Sheerin, Random neighborhood graphs as models of fracture networks on rocks: Structural and dynamical analysis, *Appl. Math. Comput.* **314**, 360 (2017).
  - [8] K. R. Gabriel and R. R. Sokal, A new statistical approach to geographic variation analysis, *Syst. Zool.* **18**, 259 (1969).
  - [9] J. N. Bandyopadhyay and S. Jalan, Universality in complex networks: Random matrix analysis, *Phys. Rev. E* **76**, 026109 (2007).
  - [10] S. Jalan and J. N. Bandyopadhyay, Random matrix analysis of network Laplacians, *Physica A (Amsterdam)* **387**, 667 (2008).
  - [11] G. Zhu, H. Yang, C. Yin, and B. Li, Localizations on complex networks, *Phys. Rev. E* **77**, 066113 (2008).
  - [12] S. Jalan, Spectral analysis of deformed random networks, *Phys. Rev. E* **80**, 046101 (2009).
  - [13] S. Jalan and J. N. Bandyopadhyay, Random matrix analysis of complex networks, *Phys. Rev. E* **76**, 046107 (2007).
  - [14] C. P. Dettmann, O. Georgiou, and G. Knight, Spectral statistics of random geometric graphs, *Europhys. Lett.* **118**, 18003 (2017).
  - [15] L. Alonso, J. A. Méndez-Bermúdez, A. González-Meléndrez, and Y. Moreno, Weighted random-geometric and random-rectangular graphs: Spectral and eigenvector properties of the adjacency matrix, *J. Complex Networks* **6**, 753 (2018).
  - [16] J. A. Méndez-Bermúdez, A. Alcazar-López, A. J. Martínez-Mendoza, F. A. Rodrigues, and T. K. DM. Peron, Universality in the spectral and eigenvector properties of random networks, *Phys. Rev. E* **91**, 032122 (2015).
  - [17] J. A. Méndez-Bermúdez, G. F. de Arruda, F. A. Rodrigues, and Y. Moreno, Scaling properties of multilayer random networks, *Phys. Rev. E* **96**, 012307 (2017).
  - [18] M. L. Mehta, *Random Matrices* (Elsevier, Amsterdam, 2004).
  - [19] E. Estrada and M. Sheerin, Random rectangular graphs, *Phys. Rev. E* **91**, 042805 (2015).
  - [20] T. A. Brody, A statistical measure for the repulsion of energy levels, *Lett. Nuovo Cimento* **7**, 482 (1973).
  - [21] T. A. Brody, J. Flores, J. B. French, P. A. Mello, A. Pandey, and S. S. M. Wong, Random-matrix physics: Spectrum and strength fluctuations, *Rev. Mod. Phys.* **53**, 385 (1981).
  - [22] F. M. Izrailev, Simple models of quantum chaos: Spectrum and eigenvectors, *Phys. Rep.* **196**, 299 (1990).
  - [23] B. Mirbach and H. J. Korsh, *Ann. Phys. (N.Y.)* **265**, 80 (1998).
  - [24] K. S. Tikhonov and A. D. Mirlin, Fractality of wave functions on a Cayley tree: Difference between tree and locally treelike graph without boundary, *Phys. Rev. B* **94**, 184203 (2016).
  - [25] I. García-Mata, O. Giraud, B. Georgeot, J. Martin, R. Dubertrand, and G. Lemarie, Scaling Theory of the Anderson Transition in Random Graphs: Ergodicity and Universality, *Phys. Rev. Lett.* **118**, 166801 (2017).
  - [26] D. A. Vega-Oliveros, J. A. Méndez-Bermúdez, and F. A. Rodrigues, Multifractality in random networks with power-law decaying bond strengths, *Phys. Rev. E* **99**, 042303 (2019).